PHYSICAL REVIEW B **82**, 041413(R) (2010)

Edge magnetotransport fingerprints in disordered graphene nanoribbons

Jean-Marie Poumirol,[1] Alessandro Cresti,[2,*] Stephan Roche,[3,4] Walter Escoffier,[1] Michel Goiran,[1] Xinran Wang,[5] Xiaolin Li,[5] Hongjie Dai,[5] and Bertrand Raquet[1]

[1]*Laboratoire National des Champs Magnétiques Intenses, INSA UPS CNRS, UPR 3228, Université de Toulouse, 143 avenue de Rangueil, 31400 Toulouse, France*

[2]*LETI, MINATEC, CEA, F38054 Grenoble, France*

[3]*INAC, SP2M, Lsim, CEA, 17 avenue des Martyrs, Grenoble, France*

[4]*CIN2, CSIC-ICN, Campus UAB, E-08193 Barcelona, Spain*

[5]*Department of Chemistry and Laboratory of Advanced Materials, Stanford University, Stanford, California 94305, USA*

(Received 13 July 2010; published 30 July 2010)

We report on (magneto)transport experiments in chemically derived narrow graphene nanoribbons under high magnetic fields (up to 60 T). Evidences of field-dependent electronic confinement are given and allow estimating the possible ribbon edge symmetry. A large positive magnetoconductance indicates a strong suppression of backscattering induced by the magnetic field. Such scenario is supported by tight-binding calculations which consider different types of underlying disorders (smooth edge disorder and long-range Coulomb scatterers).

DOI: 10.1103/PhysRevB.82.041413 PACS number(s): 72.80.Vp, 73.22.Pr, 75.47.−m

The control of the current flow in graphene nanoribbons (GNRs) constitutes a fascinating challenge for the future of carbon-based electronic devices. The description of low-energy excitations as massless Dirac fermions in graphene (resulting in large mobility at room temperature[1]), together with the possibility for band-gap engineering[2] suggest a strategy to outperform silicon devices.[3,4] However, the lateral size reduction goes along with a problematic decay of the charge mobility.[4,5] Low-temperature transport measurements on lithographically patterned GNRs unveil an ubiquitous energy gap, irrespective of the edges symmetry,[2] exceeding the confinement gap[6,7] and driven by disorder-induced charging effects.[8,9] Nonperfect edges are also expected to produce a significant scattering source. Consequences on the electronic transport have been theoretically anticipated with the formation of a mobility gap, even in the presence of an ultrasmooth edge roughness.[10] Sources of disorder such as bulk vacancies,[11] charges in the oxide,[7,9] or structural deformations[12] are also believed to alter the conductance, although the dominant scattering source remains debated. In that perspective, experimental works on narrow GNRs remain sorely lacking.

This Rapid Communication presents evidences of the one-dimensional (1D) transport character in a 11-nm-wide GNR and the possibility of tuning backscattering effects by means of an external magnetic field. Tight-binding calculations allow some assignment of the gate-dependent conductance modulations to the underlying van Hove singularities, and hence some estimation of the likely ribbon edge symmetry. The application of perpendicular high magnetic field further induces a marked enhancement of the conductance in large contrast to the magnetofingerprints of graphene flakes.[13] Close to the charge neutrality point (CNP), the measured positive magnetoconductance (MC) is attributed to the formation of the first Landau state, responsible for the closing of the energy gap and of a marked reduction in backscattering processes. Conductance simulations support the scenario of an interplay between the magnetic bands formation and a disorder-induced interband scattering suppression. Both edge disorder and long-range Coulomb scatterers yield similar conclusions.

Experiments are carried out on the first generation of chemically derived GNRs with smooth edges[14] deposited on Si/SiO_2(500 nm) wafer and connected to Pd electrodes distanced by 270 nm. Two ranges of ribbon widths are addressed: 11–30 nm and 70–100 nm. In the following, we focus on the narrow ribbons which exhibit evidence of magnetic edge currents at the root of the observed positive MC. An extended analysis of the 11-nm-wide GNR is presented. Results on the 30-nm-wide GNR are qualitatively similar. Measurements on larger GNR, here 90 nm, are briefly discussed to emphasize the effect of the electronic confinement on the MC.

Figure 1 (inset) shows the gate voltage-dependent conductance of the 11-nm-wide GNR under 50 mV bias voltage (V_b), and at various temperatures (from 169 K down to 20 K). The V-shape curves are typical for a semiconducting ribbon.[8] Interestingly, a detailed analysis of the $G(V_g)$ curves at 80 K and below unveils reproducible modulations superimposed to the overall increase in the conductance versus the electrostatic doping. These structures become more pronounced at lower bias voltages (Fig. 1 main frame, red/gray and blue/dark gray curves obtained at 50 mV and 1 mV, respectively). We assign such conductance profile to the presence of van Hove singularities (vHs), responsible for the enhancement of the backscattering in the diffusive regime. To validate such scenario, extensive tight-binding band-structures calculations are performed on a set of ribbons symmetries with varying widths.[15] Calculations include zigzag GNR (zGNR) and armchair GNR (aGNR) of three types $N=3m$, $3m+1$, and $3m+2$, N being the number of dimer lines. The N values are chosen to explore the full range of the ribbon sample width dispersion (here 11 ± 1 nm), as evaluated by careful atomic force microscopy (AFM) analysis. Figure 1 also shows the density of states $\rho(V_g)$ (dotted-dashed curve) for the armchair configuration of type $3m$ with

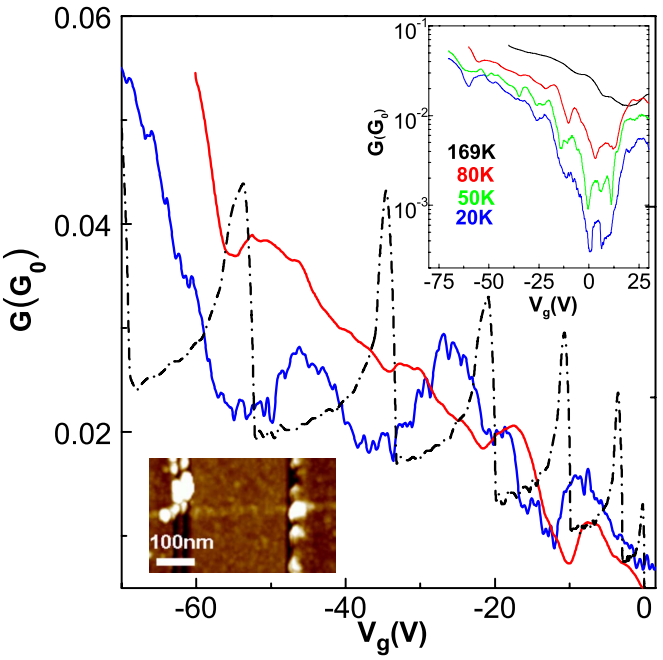

FIG. 1. (Color online) Conductance versus V_g at 80 K measured on the narrow GNR (width $\simeq$11 nm) and for two V_b, 50 mV, and 1 mV (respectively, red/gray and blue/dark gray curves). The density of states of a 90 aGNR is superimposed (dashed curve). Top inset: $G(V_g)$ at various temperatures for a wider gate voltage range. Bottom inset: AFM image of the GNR device.

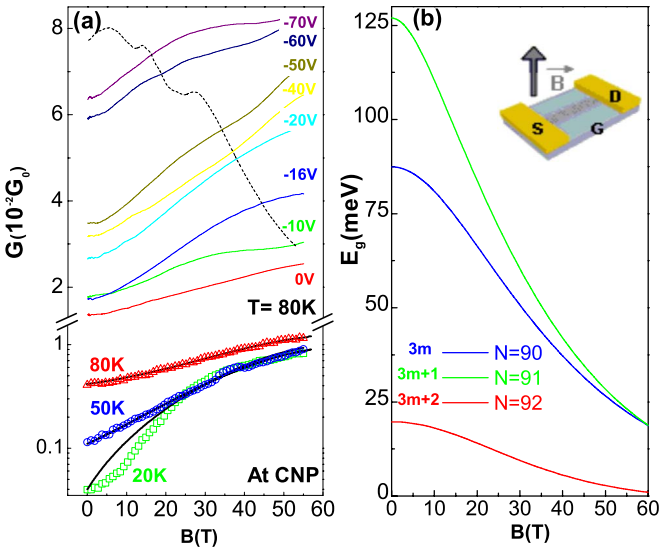

FIG. 2. (Color online) (a) Left panel: magnetoconductance at 80 K for the narrow ribbon for various V_g (top); and at 80, 50, and 20 K for V_g=0 (curves with symbols: measurements; solid lines: simulated data). The MC for a 90-nm-wide GNR is also shown, varying from $0.6G_0$ to $0.4G_0$ (dashed curve). (b) Right panel: computed field-dependent energy gaps for three different types of aGNR. Inset: schematic of the GNR device.

N=90 corresponding to a nominal width of 10.947 nm which turns out to be the most likely ribbon geometry deduced from the theoretical analysis.[15] Indeed, without any free parameters, an agreement is observed between pronounced modulations of the conductance [local minima or drastic slope changes present on the two $G(V_g)$ curves] and the theoretical sequence of the vHs. Such correspondence is not achieved at all for zGNR and other $3m+1$ and $3m+2$ types of aGNR.[15] Note that other N values, multiple of 3, from 87 to 93, in the range of the width uncertainty, also lead to a satisfactory agreement. The energies of the corresponding bands undergo a maximum shift on the order of 6%, which cannot be discriminated on the $G(V_g)$ curves. We conclude that the conductance exhibits 1D subbands fingerprints consistent with an armchair arrangement and $3m$ dimer lines (around 90 ± 3) along the GNR width.

The application of a transverse magnetic field on the 11-nm-wide GNR drastically increases its conductance by more than 50% at 80 K and by more than one decade at 20K (Fig. 2, left panel). The gain of transmission is further modulated by the electrostatic doping in a complex but very reproducible manner. The MC remains of large amplitude, even when several subbands are involved in conduction. Conversely, for a 90-nm-wide GNR [Fig. 2(a), black dashed curve] and generally speaking for graphene flakes,[16] only the very low magnetic field MC is slightly positive and results from a weak localization regime. At larger field, the conductance of large width GNR is strongly reduced, following the two-fluid model at the CNP in a diffusive regime[17] and further exhibits a steplike decrease in the quantum regime, unveiling the graphene Landau levels (LLs).[18,19] In the following, we bring evidence that the large *positive* MC and its energy dependence obtained for the narrow GNR result from a subtle interplay between the specific magnetic band structures and the field-induced reduction in disorder-driven backscattering.

The tight-binding band-structure calculations reveal that the 1D subbands of the GNR tend to the graphene LL as the magnetic field increases, since the magnetic confinement gradually overcomes the electronic one.[15] At the CNP, the onset of the zero-energy LL induces a closing of the energy band gap of the GNR. In Fig. 2(b) the simulated magnetic field dependence of the energy gaps for the three types of aGNR is reported. Assuming a flat band model at the CNP, the ribbon energy gaps $E_g(B)$ will modulate the thermally activated regime, in which the MC is expressed as $\Delta G(B) \propto \exp(-\frac{E_g(B)}{2k(T+T^*)})$. Here, kT^* accounts the kinetic-energy window of charge carriers defined by $eV_b/2$. As seen in Fig. 2(a), a reasonable agreement between experiments and the activation model is obtained, using the field dependence of the 90 aGNR tight-binding gap with $kT^* \approx 21 \pm 2$ meV, which is consistent with the 50 mV experimental V_b. We conclude that if the sequence of the vHs for an aGNR of type $3m$ appears as the most likely fingerprint of the $G(V_g)$ modulations at zero field, the agreement is further reinforced by the large positive MC.

To explore the magnetoconductance whatever the electrostatic doping, tight-binding transport simulations are performed using the Green's functions formalism and Landauer-Büttiker method.[20] In contrast to a Boltzmann transport treatment,[21] this approach includes all quantum interferences effects which are relevant for the range of parameters considered here (impurity density, mean free path, and ribbon length). Three different types of disorders are considered:

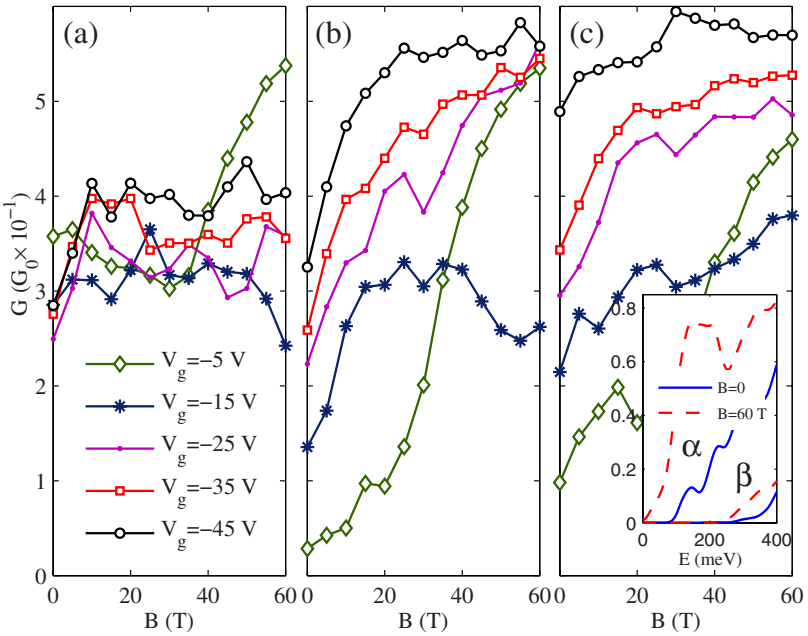

FIG. 3. (Color online) Magnetoconductance for the 90 aGNR at different V_g with (a) Anderson disorder, (b) edge roughness, and (c) Gaussian impurities. Inset of (c): α and β transmission factors denote the contributions of the first channel and the higher bands at zero field and 60 T.

the Anderson disorder (with on-site energies varying at random in the range $[-w/2,w/2]$ and $w=2$ eV); the edge roughness with a 5% of removed carbon atoms on the six outer chains at each edge; and randomly dispersed impurities described by a long-range Gaussian potential with a density 1.15×10^{16} m^{-2} (spatial range $\xi=1$ nm, strength in the range $[-u/2,u/2]$ with $u=2$ eV). These disorders are well representative of the possible scattering sources considered in the literature.[10–12] In particular, edge roughness seems unavoidable in nanoribbons, even when chemically derived;[4] whereas impurities with long-range potential mimic screened charged ions trapped in the oxide. Finally Anderson disorder qualitatively reproduces impurities on the surface of the GNR. Ripples on the ribbon surface represent another possible source of long-range disorder, but with a much weaker impact than charged impurities in the oxide.[22] The impact is even less significant in our sample, whose width is narrower than the typical ripples wavelength ($\gtrsim$15 nm). Therefore, we do not include this type of disorder in our analysis. In the following, transport calculations are performed at finite temperature $T=80$ K and for $V_b=50$ mV. A contact resistance of 10 kΩ is also included.[4]

Figure 3 shows the computed magnetoconductance at several gate voltages, for each type of disorder. First, it is clear that the use of the Anderson disorder is inappropriate to describe the experimental MC. The conductance is indeed weakly sensitive to the magnetic field (only effective at low $V_g\leq-5$ V), and this behavior hardly changes with other disorder strengths (not shown here). In contrast, a huge positive MC is observed at low V_g (where only a single conductive channel is active) for the case of edge roughness. When two or three channels are available for conduction ($V_g\sim-15$ V), the MC displays, however, a more fluctuating trend, but becomes again positive at higher gate voltages. This partially reproduces the general trend of the measured MC, suggesting that edge roughness can partly account for disorder effects but does not fully dominate the scattering processes. Finally, Gaussian disorder qualitatively reproduces the experimental trend for all V_g: the conductance increases with gate voltage and the MC is positive at almost any magnetic field and V_g values. In any case, the computed conductance remains larger than the experimental one. We demonstrate that reinforcing the disorder (its density or strength) brings the system into a strongly localized quantum regime with no well-defined positive MC.[15] Nevertheless, a more quantitative agreement between simulated and measured conductances might be achieved by considering a Gaussian disorder superimposed to an ultrasmooth edges roughness.[15]

The magnetoconductance obtained for Gaussian impurities (or edge disorder) can be further rationalized by visualizing the magnetic edge states that develop in the high magnetic field limit, as already discussed in the context of quantum wires.[23] Due to the broken time-reversal symmetry, edge channels on the upper edge are created and convey current in opposite direction than the channels at the lower edge. If disorder is not strong enough, the spatial separation between the channels induced by the high magnetic field provokes a strong suppression of backscattering. Figure 4 images the spectral current distribution at the energy $E=200$ meV for several magnetic fields. At zero magnetic field [Fig. 4(a)], the current flow is weak (as well as related conductance). Increasing B magnifies the current density along the ribbon [Figs. 4(b) and 4(c)], but the presence of scatterers limits the total current flow between source and drain. Figure 4(d) illustrates the partial backscattering along the lower edge (where electrons can only move from right to left) and partial transmission to the right contact along the upper edge (yellow arrows), when the current flow reaches a localized state. This effect is further reduced with the formation of fully developed magnetic edges at higher field [Fig. 4(e)] which further enhances the positive MC.

One notes that for the Anderson disorder, the homogeneous short-range scattering potential makes strongly difficult a spatial separation between the chiral channels, thus prohibiting the predominance of magnetic edge channels. In

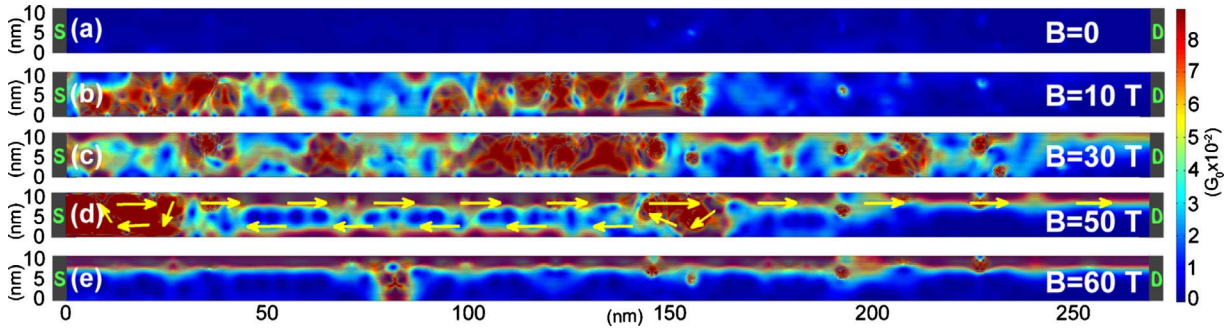

FIG. 4. (Color online) Spectral current distribution at the energy $E=200$ meV for a 90 aGNR in the presence of Gaussian disorder only at (a) $B=0$, (b) $B=10$ T, (c) $B=30$ T, (d) $B=50$ T, and (e) $B=60$ T. Charge flows from left to right.

contrast, the mechanism is efficient on the first conductive channel when bulk disorder is absent (edge roughness) or weak and long-range scattering potential prevails. In this case, intraband scattering (within the first energy band) is partially suppressed and the conductance increases as the magnetic channels are pushed to the edges. A detailed analysis disentangles the contribution of the first channel from the higher subbands (represented by the α and β factors, respectively[15]). For a Gaussian disorder, $\alpha \gg \beta$ [Fig. 3(c), inset], so the first channel dominates transport and its magnetic field dependence. The long-range nature of the Gaussian potential markedly reduces the interband scattering and preserves the positive MC of the first channel well beyond the second vHs, as observed experimentally. The higher channels are less active and do not show any marked positive MC. This is explained by the spatial enlargement of the magnetic edge states, which then come into contact more easily, due to the narrow width of the ribbon. Conversely, the short-range nature of edge disorder favors enhanced interband scattering and mixing between channels, as evident from Fig. 3(b), where the positive MC is reduced when the second and third subbands start to be involved at $V_g \simeq -15$ V.

In large magnetic field, charge-transport properties in chemically derived graphene nanoribbons can be tuned by the formation of magnetic edge states. The resulting positive magnetoconductance obtained experimentally has been further satisfactorily reproduced by tight-binding simulations, pinpointing the likely contribution of both charged impurities and smooth edge roughness.

Part of this work was supported by EuroMagNET, Contract No. 228043. S.R. acknowledges the ANR/P3N2009 (Project No. ANR-09-NANO-016-01). H.D. acknowledges funding from Office of Naval Research (ONR) and Intel.

*Current address: IMEP-LAHC, Minatec, Grenoble, France.

[1] A. K. Geim and K. Novoselov, Nature Mater. **6**, 183 (2007).
[2] M. Y. Han, B. Özyilmaz, Y. Zhang, and P. Kim, Phys. Rev. Lett. **98**, 206805 (2007).
[3] G. Liang *et al.*, IEEE Trans. Electron Devices **54**, 677 (2007).
[4] X. Wang, Y. Ouyang, X. Li, H. Wang, J. Guo, and H. Dai, Phys. Rev. Lett. **100**, 206803 (2008).
[5] Y.-M. Lin, V. Perebeinos, Z. Chen, and P. Avouris, Phys. Rev. B **78**, 161409(R) (2008).
[6] Y.-W. Son, M. L. Cohen, and S. G. Louie, Phys. Rev. Lett. **97**, 216803 (2006).
[7] C. Stampfer, J. Güttinger, S. Hellmüller, F. Molitor, K. Ensslin, and T. Ihn, Phys. Rev. Lett. **102**, 056403 (2009).
[8] M. Y. Han, J. C. Brant, and Ph. Kim, Phys. Rev. Lett. **104**, 056801 (2010).
[9] P. Gallagher, K. Todd, and D. Goldhaber-Gordon, Phys. Rev. B **81**, 115409 (2010).
[10] D. A. Areshkin, D. Gunlycke, and C. T. White, Nano Lett. **7**, 204 (2007); M. Evaldsson, I. V. Zozoulenko, H. Xu, and T. Heinzel, Phys. Rev. B **78**, 161407(R) (2008); T. C. Li and S.-P. Lu, *ibid.* **77**, 085408 (2008); E. R. Mucciolo, A. H. Castro Neto, and C. H. Lewenkopf, Phys. Rev. B **79**, 075407 (2009); D. Querlioz *et al.*, Appl. Phys. Lett. **92**, 042108 (2008); A. Cresti *et al.*, Nano Res. **1**, 361 (2008); P. Zhao *et al.*, *ibid.* **1**, 395 (2008).
[11] S. Ihnatsenka and G. Kirczenow, Phys. Rev. B **80**, 201407(R)(2009).
[12] M. I. Katsnelson and A. K. Geim, Philos. Trans. R. Soc. A **366**, 195 (2008).
[13] K. Novoselov *et al.*, Nat. Phys. **2**, 177 (2006); X. Wu, X. Li, Z. Song, C. Berger, and W. A. de Heer, Phys. Rev. Lett. **98**, 136801 (2007).
[14] X. Li *et al.*, Science **319**, 1229 (2008).
[15] See supplementary material at http://link.aps.org/supplemental/10.1103/PhysRevB.82.041413 for details of the conductance simulations and supplementary experimental data.
[16] F. V. Tikhonenko, D. W. Horsell, R. V. Gorbachev, and A. K. Savchenko, Phys. Rev. Lett. **100**, 056802 (2008).
[17] S. Cho and M. S. Fuhrer, Phys. Rev. B **77**, 081402(R) (2008).
[18] V. P. Gusynin and S. G. Sharapov, Phys. Rev. B **71**, 125124 (2005).
[19] T. S. Li *et al.*, Philos. Mag. **89**, 697 (2009).
[20] A. Cresti *et al.*, Eur. J. Phys. B **53**, 537 (2006).
[21] S. Adam *et al.*, Proc. Natl. Acad. Sci. U.S.A. **104**, 18392 (2007).
[22] A. Deshpande, W. Bao, F. Miao, C. N. Lau, and B. J. LeRoy, Phys. Rev. B **79**, 205411 (2009); Y. Zhang *et al.*, Nat. Phys. **5**, 722 (2009); J. H. Chen *et al.*, Solid State Commun. **149**, 1080 (2009).
[23] A. Cresti, G. Grosso, and G. P. Parravicini, Phys. Rev. B **77**, 115408 (2008).